Soluble fullerene derivatives

Ball, James M.; Bouwer, Ricardo K.M.; Kooistra, Floris B.; Frost, Jarvist M.; Qi, Yabing; Buchaca Domingo, Ester; Smith, Jeremy; de Leeuw, Dago M.; Hummelen, Jan C.; Nelson, Jenny

Published in:
Journal of Applied Physics

DOI:
10.1063/1.3605531

Publication date:
2011

Soluble fullerene derivatives: The effect of electronic structure on transistor performance and air stability

James M. Ball,[1] Ricardo K. M. Bouwer,[2,3] Floris B. Kooistra,[2,4] Jarvist M. Frost,[1] Yabing Qi,[5] Ester Buchaca Domingo,[6] Jeremy Smith,[1] Dago M. de Leeuw,[7] Jan C. Hummelen,[2,4] Jenny Nelson,[1] Antoine Kahn,[5] Natalie Stingelin,[6] Donal D. C. Bradley,[1] and Thomas D. Anthopoulos[1,a)]

[1]*Department of Physics, The Blackett Laboratory, Imperial College London, London, SW7 2AZ, United Kingdom*
[2]*Stratingh Institute for Molecular Chemistry, University of Groningen, Nijenborgh 4, 9747 AG, Groningen, The Netherlands*
[3]*Dutch Polymer Institute, PO Box 902, 56000 AX Eindhoven, The Netherlands*
[4]*Zernike Institute for Advanced Materials, University of Groningen, Nijenborgh 4, 9747 AG, Groningen, The Netherlands*
[5]*Department of Electrical Engineering, Princeton University, Princeton, New Jersey 08544, USA*
[6]*Department of Materials, Imperial College London, London, SW7 2AZ, United Kingdom*
[7]*Phillips Research Laboratories, High Tech Campus 4, Eindhoven, Newfoundland and Labrador-5656AE, The Netherlands*

(Received 15 March 2011; accepted 18 May 2011; published online 8 July 2011)

The family of soluble fullerene derivatives comprises a widely studied group of electron transporting molecules for use in organic electronic and optoelectronic devices. For electronic applications, electron transporting (n-channel) materials are required for implementation into organic complementary logic circuit architectures. To date, few soluble candidate materials have been studied that fulfill the stringent requirements of high carrier mobility and air stability. Here we present a study of three soluble fullerenes with varying electron affinity to assess the impact of electronic structure on device performance and air stability. Through theoretical and experimental analysis of the electronic structure, characterization of thin-film structure, and characterization of transistor device properties we find that the air stability of the present series of fullerenes not only depends on the absolute electron affinity of the semiconductor but also on the disorder within the thin-film. © *2011 American Institute of Physics*. [doi:10.1063/1.3605531]

I. INTRODUCTION

Exploiting the potential of solution processable organic field-effect transistors (OFETs) for low-cost logic applications has been an ambition of the organic semiconductor research community for several years. To optimize the speed, stability, and power consumption of organic logic circuits a complementary device architecture is used, which requires both n- and p-channel (electron and hole transporting) organic semiconductors.[1,2] To minimize costs both commercially and for researchers, using air-stable semiconductor materials circumvents the necessity for fabrication under inert atmospheric conditions and/or additional encapsulation layers. Previous efforts in the development of air-stable p-channel organic semiconductors have yielded high performance materials.[3–5] However, producing solution processable air-stable n-channel devices with equivalent performance has only been achieved in the last few years[6–8] and remains challenging for many families of materials.

Improving the air stability of electron transporting solution processable organic semiconductors has proven to be a difficult problem to overcome. The current understanding of the origin of atmospheric instability of n-channel materials is that mobility degradation is a result of electron trapping by adsorbed atmospheric oxidants,[9–11] namely water and oxygen. Stability is therefore determined by the molecular orbital energetics of the semiconductor[10–12] and morphological kinetic barriers[10,13] against oxidant diffusion. Both analyses in the literature[11] and empirical studies[10,12] have concluded that if the LUMO level of the semiconductor can be lowered below the trap energy of atmospheric oxidants then the semiconductor anionic species should be stable against electron trapping. In particular, an analysis by Jones *et al.*[10] concluded that the rate of degradation in a series of arylene diimides upon atmospheric exposure scales with electron affinity up to ~4.3 eV (obtained by solution phase electrochemical measurements) at which point long term stabilization is possible. Usta *et al.*[12] found that the onset of stabilization was achieved at an electron affinity in the range of 4.0–4.1 eV.

One family of electron-transporting carbon-based semiconductors that has received significant attention is the fullerenes. Thin-films of insoluble C_{60} have been found to exhibit a high field-effect electron mobility of up to 6 cm^2/Vs.[14,15] Chemical derivation of the parent carbon cage has yielded soluble fullerene derivatives that have been successfully used in electronic[16–22] and optoelectronic[23–28] devices as electron transporting/accepting materials. Previous work on improving the stability of fullerene derivatives in transistors has focused on chemical doping to increase the mobile charge density[29] or

a)Author to whom correspondence should be addressed. Electronic mail: thomas.anthopoulos@imperial.ac.uk.

modifying the side-group to produce a kinetic barrier to oxidant diffusion. Specifically the introduction of fluorocarbon side-chains was found by both Wöbkenberg *et al.*[20] and Chikamatsu *et al.*[19] to yield improved stability of OFET performance in comparison with 6,6-phenyl-C_{61}-butyric acid methyl ester ([60]PCBM), the widely studied benchmark fullerene (Fig. 1(a)). The use of fluorocarbon as opposed to hydrocarbon side chains is thought to improve air stability by reducing the free volume through which oxidants can diffuse to the channel due to the increased van der Waals radius of fluorine,[10] by increasing hydrophobicity to limit water diffusion, and/or by increasing thin-film crystallinity.[19] However, direct chemical modification of the carbon cage to increase the electron affinity of fullerenes derived from C_{60} is yet to be investigated with regards to air-stability.

The soluble PCBM derivative of C_{84} has been shown to exhibit improved air-stability in comparison to its C_{60} analog as a result of its higher electron affinity.[30] However, the low production yield currently limits application of the molecule. Previously, Brabec *et al.*[31] used a series of C_{60} derivatives for investigation of the effect of the LUMO level of the acceptor on the open circuit voltage (V_{OC}) in bulk heterojunction (BHJ) solar cells. They concluded that the off-set between the donor HOMO and the acceptor LUMO plays an important role.[31] In their study they used the soluble quasifullerene *N*-3-(2-ethylhexyloxy)benzyl ketolactam (Ketolactam-1, Fig. 1(b)). The authors reported that this chemical change to the structure of the cage resulted in an increase of the electron affinity of the fullerene relative to [60]PCBM. However, increasing V_{OC} in BHJ solar cells is achieved by lowering the electron affinity of the acceptor. One fullerene that has received recent attention toward this aim is the bis-adduct of PCBM (bis-PCBM, Fig. 1(c)).[32–35] These two materials are therefore useful for extending the range of LUMO levels of fullerenes for the current investigation and may also give insight into degradation mechanisms applicable to BHJ solar cells.

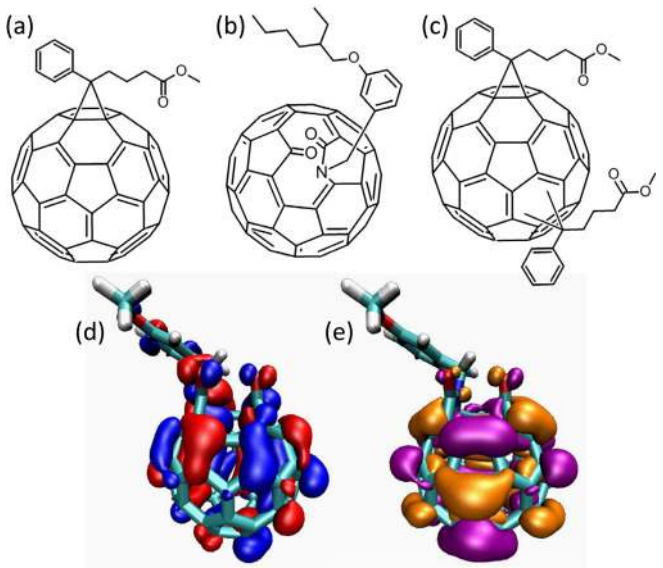

FIG. 1. (Color online) Chemical structures of (a) [60]PCBM, (b) Ketolactam-1, and (c) bis-PCBM (one possible isomer). (d) HOMO and (e) LUMO spin densities for a ketolactam quasifullerene (equivalent to Ketolactam-1 with a truncated alkyl side chain) as calculated by DFT.

In the present paper we study a series of three soluble fullerenes with different electronic structures and investigate structural effects on air stability in this family of materials. We present data on the electronic structure of fullerene derivatives based on density functional theory (DFT) calculation of isolated molecules; ultraviolet photoelectron spectroscopy (UPS), and inverse photoemission spectroscopy (IPES) of solid state films; and solution phase cyclic voltammetry (CV). The impact of the electronic structure modification on device performance is assessed. Thin-film characterization by atomic force microscopy (AFM) and differential scanning calorimetry (DSC) suggest only minor microstructural differences in films as deposited from solution despite differences emerging following thermal treatment. Water contact angle measurements suggest negligible differences in hydrophobicity between the fullerene thin-films. Finally, temperature-dependent charge transport measurements suggest that the extent of energetic disorder in the semiconductor plays an important role in determining the atmospheric stability of these fullerenes. On the basis of stability and charge transport studies we conclude that the energy required for hopping between localized semiconductor states relative to the energy required for hopping into a trap state determines the relative anionic stability against electron trapping by atmospheric oxidants in the present group of fullerenes.

II. EXPERIMENTAL METHODS

A. Transistor fabrication and characterization

Bottom-gate, top-contact transistors were fabricated on doped Si wafers that served as both the substrate and the gate electrode with a thermally grown 400 nm SiO_2 insulating layer. The gate oxide was passivated[22] by spin-coating a solution of divinyltetramethyl disiloxane-bis(benzocyclobutene) (BCB) diluted at a ratio of 1:20 (by volume) in trimethylbenzene at 3000 rpm followed by thermal annealing at 250 °C for 1 h under N_2. The oxide-polymer composite gate insulator has a calculated geometric capacitance (C_i) of 7.7 nF/cm^2 ($C_{BCB} = 71.4$ nF/cm^2 and $C_{silica} = 8.6$ nF/cm^2).[22] Fullerenes were spin cast onto the composite dielectric from 1 wt. % chlorobenzene solutions (filtered through a 0.2 μm PTFE filter) under N_2. Devices were completed following shadow mask evaporation of Au or Al source and drain contact electrodes under vacuum. Basic transistor measurements were conducted under N_2. Samples were transferred to a vacuum probe station ($\sim 10^{-5}$ mbar) for temperature-dependent charge transport measurements and were left under vacuum for a minimum of 12 h before commencing measurements to ensure desorption of impurities. Air stability measurements were performed in the laboratory atmosphere with humidity and temperature maintained at ~30% and ~19 °C respectively. Current-voltage measurements were performed using a Keithley 4200-SC Semiconductor Parameter Analyzer.

B. Electronic structure determination

Fullerene thin-films (with a thickness of ~ 20 nm) were prepared for UPS/IPES by spin coating 10 mg/ml solutions of

each material in chlorobenzene onto cleaned ITO glass substrates. The samples were packaged under N_2 at Imperial College London and sent to Princeton University for electronic structure determination. The samples were transferred to an ultrahigh vacuum system (base pressure $= 2 \times 10^{-10}$ Torr) for UPS/IPES measurements. A He discharge lamp was used as the UV light source and both UPS He I ($h\upsilon = 21.22$ eV) and He II ($h\upsilon = 40.81$ eV) data were collected. For IPES measurements, to minimize beam damage, data were collected from 9 different spots on the samples and averaged. Measurement uncertainties are 0.15 eV for UPS and 0.45 eV for IPES.

Cyclic voltammetry was performed using an Autolab PGStat100 with platinum working and counter electrodes and a silver reference electrode. The voltage was measured (scan rate 10 mV/s) for a solution of each material in *ortho*-dichlorobenzene:acetonitrile (4:1) relative to ferrocene (Fc/Fc^+) using Bu_4NPF_6 (0.1 M) as the supporting electrolyte. Analyte concentrations were typically $\sim 10^{-3}$ M.

C. Thin-film characterization

For thermal analysis, thin-films of the fullerene derivatives were produced by preparing homogeneous solutions of each fullerene at 1 wt. % in chlorobenzene followed by drop casting onto a clean glass substrate. The solvent was evaporated at ambient leaving 1–5 mg of material to be used for the differential scanning calorimetry (DSC) experiments. These measurements were conducted under nitrogen at a scan rate of 10 °C/min using a Mettler Toledo DSC822.

AFM (Pacific Nanotechnology) measurements were performed in the channel of transistor structures prepared as described above. Measurements were performed in ambient atmosphere.

Water contact angle measurements were performed on spin-cast fullerene thin-films following the same fabrication procedure as used for OFETs. Measurements were performed using a Krüss Drop Shape Analysis system in air with humidity and temperature maintained at ~40% and ~20 °C, respectively.

III. RESULTS AND DISCUSSION

A. Electronic structure of fullerenes

Figure 1 shows the molecular structure of the three fullerenes used in the present study. The relief of strain is the main driving force for additions to fullerenes, so chemical changes to the cage alters both their symmetry and the carbon-carbon bond lengths. This results in a modification of the electronic structure.[36] The three derivatives each have different or multiple side-chain bonding, hence, different molecular orbital energies. Ground state DFT calculations were performed to obtain the electronic structure of a single molecule of each material given in Fig. 1. The calculated energetic positions of the highest occupied (HO) and lowest unoccupied (LU) molecular orbital (MO) are summarized in Table I. Experimentally bis-PCBM is processed as an isomeric mixture.[35] The values quoted are the mean MO energies accounting for all structural isomers.[34] The LUMO is derived by adding the energy of the first singlet excitation calculated using time-dependent DFT (b3lyp/6-31 g*) to the energy of the HOMO calculated from hybrid DFT (b3lyp/6-31 g*). Further details on the calculation method have been published elsewhere.[34] The calculations suggest that this series of fullerenes exhibits an increasing electron affinity from bis-PCBM to [60]PCBM to Ketolactam-1. The frontier orbital spin densities for a ketolactam quasifullerene with an equivalent cage structure to Ketolactam-1 and truncated side-chain are shown in Figs. 1(d) and 1(e). The HOMO spin density indicates regions of accessible oxidation. The LUMO spin density indicates regions of oxidation or trapping of the charge transporting anion. Increasing the length of the alkyl side-chain was found to have no effect on the calculated MO energies.

Both solution phase cyclic voltammetry (CV) and UPS/IPES measurements in the solid state were used for experimental estimation of the MO energies. It should be emphasized that the DFT calculation is based on an isolated molecule in vacuum at 0 K. Both temperature and the surrounding medium may influence the experimental measurements. Therefore, only trends in electronic structure variation by cage modification will be compared between experiment and calculation and not the absolute values for a particular fullerene. The results of CV measurements to obtain the first reduction potential of each fullerene are summarized in Table I. The LUMO levels of mono- and bis-PCBM are obtained by assuming[37] $E_{LUMO} = -(4.8 + E_{red})$, where 4.8 eV is the ionization potential of Fc/Fc^+. The LUMO level of Ketolactam-1 is obtained assuming a difference in reduction potential relative to [60]PCBM, as given by Ref. 31. Good agreement in the trend of increasing electron affinity of the fullerenes between calculation and experiment is obtained.

Solid thin-films were prepared for UPS/IPES measurements by spin coating each semiconductor onto clean ITO

TABLE I. Summary of material and device parameters. μ_{sat} and V_T were extracted from devices with $L = 20$ μm, $W = 1500$ μm and Al top contact electrodes at $V_D = 50$ V. Mobility as a function of exposure time ($\mu_{t>0}$) was extracted from devices with $L = 50$ μm, $W = 1500$ μm and Au top contact electrodes at $V_D = 50$ V

Molecule	HOMO (eV)			LUMO (eV)			μ_{sat} (cm^2/Vs)	V_T (V)	Time (min) for $\mu_{t>0} = 0.1\mu_{t=0}$
	DFT	UPS	CV	DFT	IPES	CV			
[60]PCBM	−5.6	−5.8	-	−3.7	−3.80	−3.72	0.09	9.0	~390
Ketolactam-1	−5.9	−6.0	-	−4.0	−4.17	−3.89[a]	0.008	5.8	~520
bis-PCBM	−5.5	−6.0	-	−3.6	−3.6	−3.60	0.003	5.8	~4

[a]Ref. 31

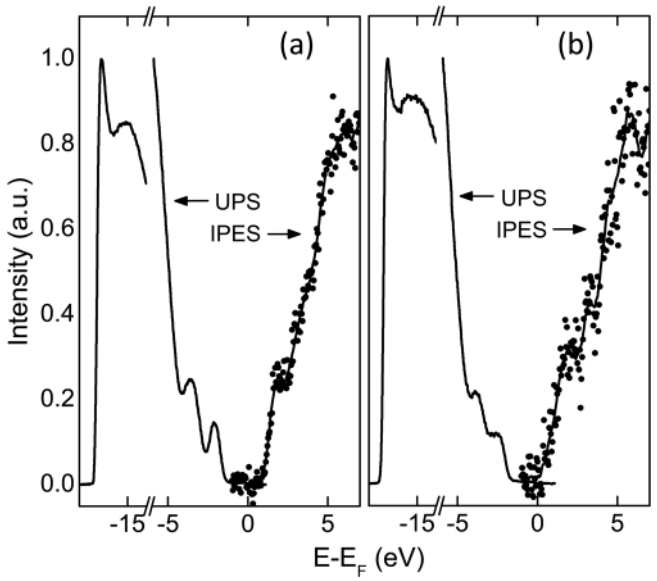

FIG. 2. Ultraviolet photoelectron spectra (UPS) and inverse photoemission spectra (IPES) taken from thin-films of (a) bis-PCBM and (b) Ketolactam-1 for experimental determination of the electronic structure of fullerenes.

coated glass substrates. The spectral data from measurements of Ketolactam-1 and bis-PCBM are shown in Fig. 2 and the extracted energetic positions of the HOMO and LUMO are given in Table I. The UPS/IPES peaks associated with the occupied and unoccupied molecular orbitals are broadened as a result of static and dynamic disorder in the solid state. The states at the edge of the HOMO and LUMO distributions are of most relevance to charge transport. Therefore, the HOMO and LUMO energies are estimated from the onset of the closest peak to the Fermi level in the photoelectron and inverse photoemission spectra, respectively. The results obtained from [60]PCBM compare favorably with a previous study employing the same techniques.[38] The same trend in increasing electron affinity as observed in DFT and CV results is obtained with IPES measurements. Interestingly, the LUMO level of Ketolactam-1 measured using this method is comparable to the onset electron affinity previously reported as a requirement for air-stable electron transport.[10,12]

B. Thin-film characterization

Following estimation of the electronic structure of the fullerenes, a series of thermal and microstructural analyses were conducted to assess any possible differences in thin-film morphology that may influence either charge transport or air stability. AFM was used to assess the thicknesses as well as any differences in the surface morphology between the fullerene films. AFM images of thin-films of each of the three fullerenes spin-cast from 1 wt. % chlorobenzene solutions are shown in Fig. 3. The thin-film thicknesses were estimated to be 36 nm, 29 nm, and 54 nm for [60]PCBM, Ketolactam-1, and bis-PCBM, respectively. Furthermore, all three show a similar smooth and uniform surface with no discernable features. RMS roughness values for [60]PCBM, Ketolactam-1, and bis-PCBM thin-films were measured to be 0.21 nm, 0.23 nm, and 0.35 nm, respectively. The kinetic barrier afforded by close packing in a crystalline structure[10,19] and the consequences of trapping at grain boundaries[13] have been suggested to be important parameters affecting air stability. However, the AFM images show no obvious features that could be related to crystalline structure or obvious differences in the density of grain boundaries for any of the fullerenes. This suggests the kinetic barrier will not be a significant variable when comparing air stabilities.

Complementary to AFM, DSC was also performed on solid films of each fullerene to obtain a more quantitative picture of both the overall degree of crystallinity and the thermal behavior of the three fullerenes when deposited from solution. The thermal behavior of fullerenes is also of relevance to other fields, e.g., for the fabrication of high efficiency organic BHJ solar cells.[25,39] Films were initially drop cast onto glass substrates from 1 wt. % chlorobenzene solutions and then transferred to a DSC crucible for thermal analysis. Although the drop cast films may be morphologically different from the spin cast films, this data should be indicative of the relative ability of each fullerene to form crystalline structures from chlorobenzene solutions.

The first heating and cooling thermograms for each material are shown in Fig. 4. A conspicuous difference in the thermal behavior was found for the three fullerenes. Solution cast [60]PCBM initially formed a predominantly amorphous structure that recrystallizes upon heating. This is evident from the exothermic transition at ~190 °C observed in the first heating cycle. A pronounced melting endotherm of the crystalline [60]PCBM phase is found at ~280 °C with a corresponding enthalpy of fusion of 14.44 J/g. Previous DSC analysis of [60]PCBM obtained identical features in the first cooling and second heating cycles.[40] In comparison, both bis-PCBM and Ketolactam-1 seem to feature a significantly lower degree of crystallinity, below the DSC detection limit (< 10%). As an isomeric mixture, films of bis-PCBM are expected to be non-crystalline. During the first heating cycle both bis-PCBM and Ketolactam-1 exhibit broad endothermic changes which we tentatively attribute to the removal of residual solvent as these features do not occur for subsequent

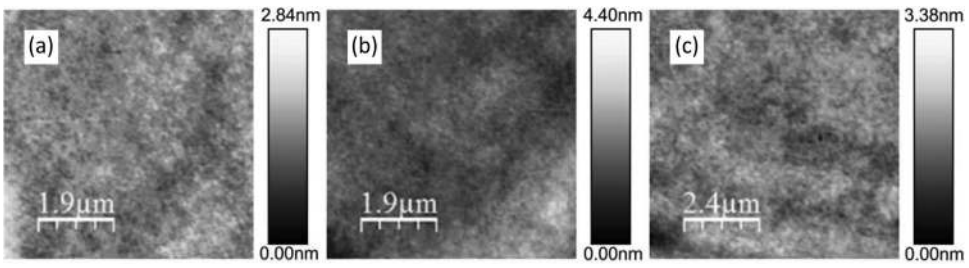

FIG. 3. AFM images of thin films of (a) [60]PCBM, (b) Ketolactam-1, and (c) bis-PCBM.

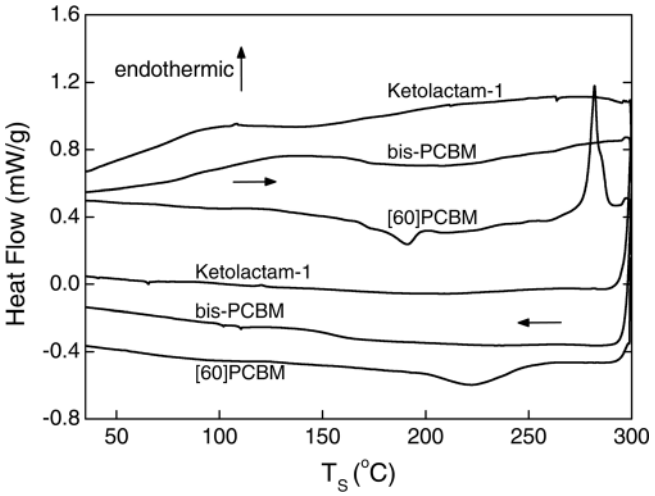

FIG. 4. DSC thermograms during the first heating and cooling cycles obtained from drop-cast material of each of the three fullerenes studied here. The enthalpy of fusion for [60]PCBM is deduced from the area under the melting endotherm.

heating cycles. For bis-PCBM and Ketolactam-1, the second and third heating cycles show glass transitions at ~165 °C and ~100 °C, respectively. The DSC data thus suggest that *as-cast* thin-films of all three materials are of a relatively low degree of crystallinity. Therefore, the relative crystallinity of such as-cast films is unlikely to be a variable when comparing air stability.

The contact angles of sessile water drops were measured on the fullerene thin-films to compare their hydrophobicities. Contact angles of 89°, 87°, and 89° were obtained on [60]PCBM, Ketolactam-1, and bis-PCBM respectively. This suggests that water diffusion into the channel may be limited by its weak interaction with the fullerenes, but similarly so for each material. This may reduce the rate of transistor degradation resulting from electron trapping by water. The high water contact angle observed for Ketolactam-1 may be surprising given that the oxygen atoms in the ketolactam group are expected to be hydrogen bond acceptors. The result suggests this group does not dominate the macroscopic interaction of Ketolactam-1 films with water.

C. Field-effect transistors measurements

Having established the differences in electronic structure but similarities in thin-film morphology for the three fullerenes investigated here we fabricated OFETs with a bottom-gate, top-contact (BGTC) architecture (see the inset of Fig. 5). The transfer and output characteristics of devices based on the three fullerenes using Al source and drain electrodes are shown in Fig. 5. All three show hysteresis-free current-voltage characteristics. The saturation electron mobility (μ_{sat}) and threshold voltage (V_T) are calculated from a linear fit of the square-root of the drain current ($I_D^{1/2}$) as a function of gate voltage (V_G) according to

$$I_D = \mu_{sat} W C_i (V_G - V_T)^2 / 2L, \quad (1)$$

where W and L are the transistor channel width and length, respectively. The extracted device parameters are summarized in Table I. The values of μ_{sat} and threshold charge density, $C_i V_T$, for [60]PCBM are comparable to previous reports with similar device architectures.[21,22] The output characteristics in Fig. 5 show a linear increase in I_D at increasing low V_D suggesting Ohmic injection with Al contacts. When using Au contacts, qualitatively, equivalent behavior is observed.

The observation of Ohmic contacts with respect to the lateral field and the absence of long-range crystallinity allows the use of the transmission line method[41,42] to quantify the contact resistance ($R_{Contact} = R_{Source} + R_{Drain}$). Assuming the resistance of the contacts is in series with that of the OFET channel ($R_{Channel}$), the transmission line method allows extraction of $R_{Contact}$ using a linear extrapolation of the total device resistance of a series of transistors of varying channel length (but fixed width, $W = 1500$ μm) to $L = 0$ μm (i.e., $R_{Channel} = 0$ Ω). An example of the use of the method is shown in Fig. 6(a), where the y-axis intercept of each linear fit determines $R_{Contact}$ at different values of gate bias. The

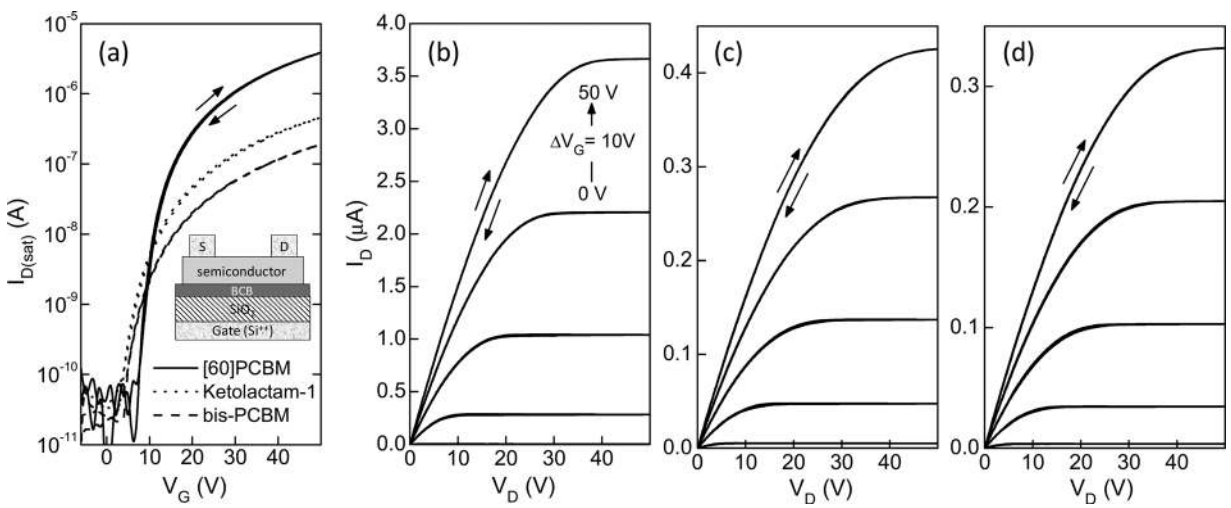

FIG. 5. Transistor characteristics obtained from bottom gate top contact (Al) transistors. $W = 1500$ μm and $L = 200$ μm. (a) Saturation regime transfer characteristics at $V_D = 50$ V for all three fullerenes (inset: device structure used in the present study). Output characteristics of the same devices using (b) [60]PCBM, (c) Ketolactam-1, and (d) bis-PCBM.

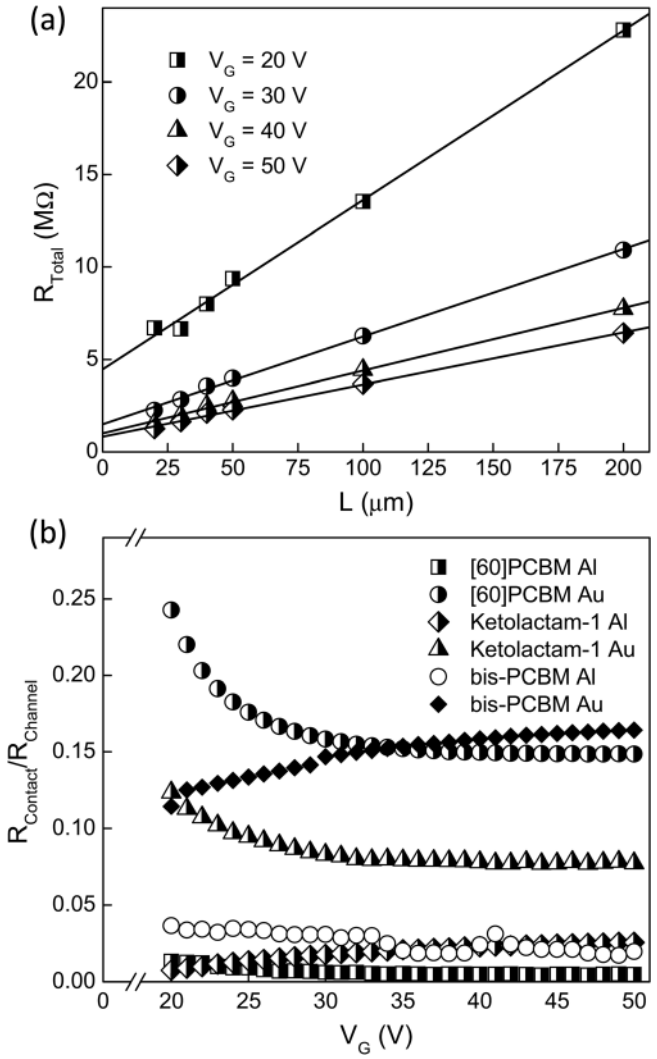

FIG. 6. (a) Example plot of transmission line method extraction of contact resistance using transistors based on [60]PCBM with Au top contacts ($L = 200$ μm, $W = 1500$ μm). (b) $R_{Contact}/R_{Channel}$ ratio for each semiconductor/electrode system investigated in this report ($L = 200$ μm, $W = 1500$ μm).

energetic barrier to electron injection from the Fermi level of the metal to the LUMO level of the semiconductor is expected to contribute to the contact resistance.[43,44] Additionally, in a BGTC transistor architecture, any space-charge effect resulting from charge transport through the thickness of the semiconductor layer beneath the contact will also contribute to the measured contact resistance following this method. Because each fullerene has a different electronic structure and mobility, these effects are difficult to disentangle in this instance. In an attempt to minimize the contribution of the mobility we use the ratio of $R_{Contact}/R_{Channel}$ as our figure of merit. This is shown in Fig. 6(b) for each device structure studied here as a function of gate bias for transistors of length $L = 200$ μm. Figure 6(b) indicates that the values for $R_{Contact}/R_{Channel}$ are much less than 1 in this device geometry. This suggests that the I-V characteristics of the devices are dominated by the semiconducting channel as opposed to the contacts. As the channel length decreases (not shown) the resistive contribution due to the contacts does become significant with respect to the total device resistance.

When using different electrode metals for the same fullerene, one observes that increasing the work function ($\varphi_{Al} = 4.2$ eV to $\varphi_{Au} = 5.0$ eV) increases the $R_{Contact}/R_{Channel}$ ratio in agreement with an increased barrier to electron injection into the LUMO level of the semiconductor. The equivalent result has been observed previously in [60]PCBM.[21,22] However, a comparison of the resistance ratio between different fullerenes is more subtle. In particular, bis-PCBM is expected to exhibit an increased $R_{Contact}/R_{Channel}$ ratio in comparison to the other fullerenes, which we do not observe for all voltages. Additional details of the injection interface, such as variations in the metal penetration into the semiconductor during top contact deposition[45] and dipole formation at the metal-fullerene interface modifying the effective injection barrier[46] may be influencing these results, among other effects.[44] Further analysis of the charge injection/extraction mechanism is clearly required for a full understanding of this discrepancy but is beyond the scope of the current report and will not be addressed further here.

D. Air stability of fullerene transistors

Following OFET characterization, the air stability of each fullerene film was assessed using the transistor transfer characteristics as a function of atmospheric exposure time. The measurements were carried out in the dark with humidity and temperature maintained at ~30% and ~19 °C respectively. The device structure was equivalent to the previous OFET measurements, using stable Au source and drain electrodes to avoid degradation of the device performance due to instability of the contacts. Degradation of the device characteristics due specifically to injection instability, i.e., contact resistance as a function of exposure time, could not be explicitly monitored using the present method. This is because the time scale required for many discrete transmission line measurements exceeds the time scale over which degradation occurs at early stages of the experiment.

Figure 7(a) shows the mobility in the saturation regime as a function of exposure time ($\mu_{t>0}$) normalized to the saturation mobility as measured under inert conditions ($\mu_{t=0}$) for all three fullerenes. All fullerenes studied here suffer from mobility degradation as a function of exposure time. Bis-PCBM, with the lowest electron affinity, exhibits the fastest mobility degradation upon atmospheric exposure, in agreement with the hypothesis that the LUMO level off-set with the reduction potential of atmospheric oxidants determines air stability. Ketolactam-1, with the deepest LUMO level, is also unstable despite the observation of a comparable electron affinity required for stabilization as obtained in Ref. 12. Both [60]PCBM and Ketolactam-1 show a similar degradation as a function of exposure time (Ketolactam-1 degrades slightly slower) despite the experimentally obtained difference in electron affinity of ~0.3 eV. This is surprising given that the material characterization suggests little difference in the kinetic barrier between the films. However, because the electron mobilities in these two materials differ by a factor of ten, the discrepancy between the result and hypothesis may be related to the charge transport mechanism.

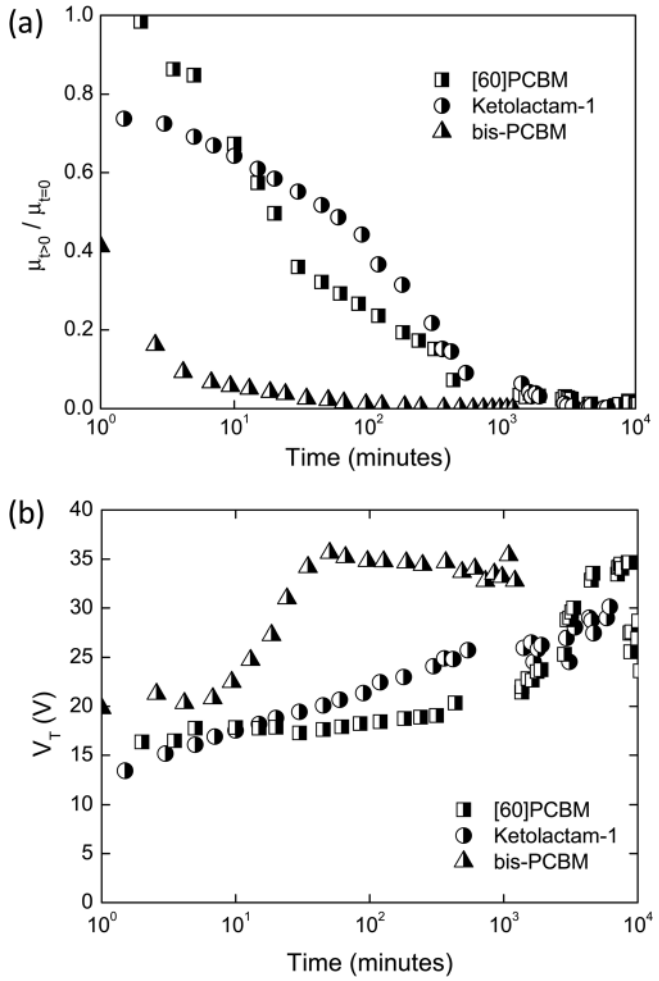

FIG. 7. Air stability of fullerenes. (a) Saturation mobility ($V_D = 50$ V) as a function of atmospheric exposure time ($\mu_{t>0}$) normalized to the saturation mobility measured under inert conditions ($\mu_{t=0}$). (b) Threshold voltage as a function of atmospheric exposure time.

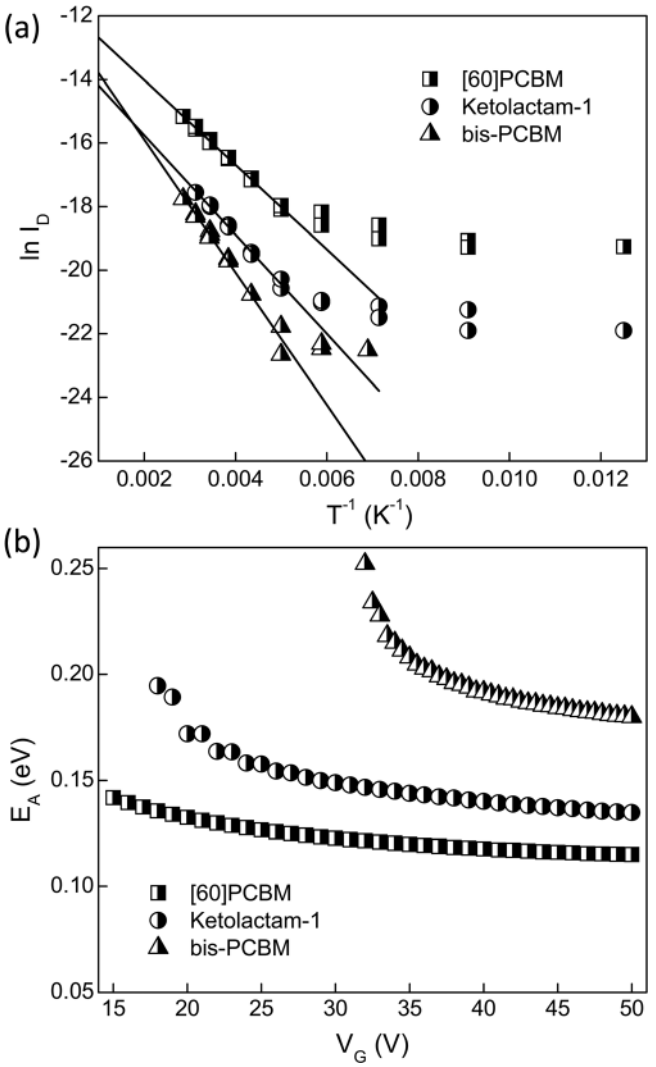

FIG. 8. (a) Arrhenius plots of the linear regime drain current ($V_D = 1$ V, $V_G = 50$ V) for all three fullerenes. Lines are best fits for the extraction of the activation energy in the moderate temperature region. (b) Gate voltage dependence of the activation energy (moderate temperature) of the drain current in the linear regime.

Figure 7(b) indicates that the threshold voltage in OFETs based on all three fullerenes increases with exposure time to air. This suggests that atmospheric oxidants act as deep traps, which render an increasing density of carriers immobile with increasing exposure time. V_T appears to saturate for bis-PCBM at exposure times > 100 min. The origin of this behavior is unclear. The change in V_T increases from [60]PCBM to Ketolactam-1 to bis-PCBM. OFETs based on bis-PCBM may be expected to exhibit the greatest change in V_T, where for a given trap density a relatively larger proportion of transport states will be inaccessible due to the raised LUMO relative to the other fullerenes. However, the same argument would suggest that the observed change in V_T in OFETs based on Ketolactam-1 and [60]PCBM should be reversed. Again, this may be related to the charge transport mechanism in these materials.

E. Charge transport in fullerene transistors

Charge transport in the fullerene-based OFETs was assessed using temperature (T)-dependent current-voltage measurements performed under vacuum. All temperature-dependent measurements used transistors with a channel length of $L = 200$ μm and Al contact electrodes to minimize the influence of contact resistance (see Fig. 6(b)). An example Arrhenius plot shown in Fig. 8(a) describes the temperature dependence of I_D at $V_G = 50$ V and $V_D = 1$ V (linear regime) according to

$$\ln I_D = -(E_A/K_B T) + \ln I_{D,0}, \tag{2}$$

where E_A is the activation energy, K_B is Boltzmann's constant, and $I_{D,0}$ is the current prefactor (I_D for $T \to \infty$). Measurements are included in Fig. 8(a) for decreasing and then increasing temperature. The graph shows two distinct regions, which shall be referred to as the moderate temperature ($350\ \text{K} > T > 200\ \text{K}$) and low temperature ($T < 200$ K) regions. The linear fit to the moderate temperature region is indicative of thermally-activated hopping transport and has been observed previously in both soluble fullerenes[47,48] and evaporated C_{60} films.[49] The low temperature regime, where the current becomes almost temperature independent, is typically attributed to transport dominated by tunneling.

Figure 8(b) shows the activation energy at moderate temperatures extracted from Arrhenius plots of I_D in the linear regime as a function gate bias. The measured activation energy is a function of the average energy required for a charge carrier to hop from one transport site to the next. Qualitatively, in an energetically and spatially disordered system with either a Gaussian or exponential localized density of states (DOS) distribution the activation energy for hopping will depend on the induced charge density. Upon increasing the gate bias an increasing number of carriers populate the DOS and more sites become thermally accessible. This decreases the average activation energy. The rate of decrease will depend on the energetic distribution of localized states which in general is unknown.

Bis-PCBM is processed as an isomeric mixture and with its additional side-chain is expected to form films with increased energetic disorder and reduced packing density in comparison with [60]PCBM and Ketolactam-1. It is therefore unsurprising to observe higher activation energies for transport in films of this material. Increased energetic disorder may be expected to broaden the DOS distribution resulting in larger changes in E_A as the charge density in the channel increases. Lenes *et al*. also concluded that the origin of the decrease in the current in diodes using bis-PCBM compared to [60]PCBM was a result of broadening of the DOS.[33]

The origin of the difference in E_A between Ketolactam-1 and [60]PCBM is not immediately clear. As both molecules have a similarly sized side-chain and form apparently amorphous films on deposition from solution, the difference may be a result of distortion of the LUMO causing a reduction in intermolecular orbital coupling. However, the values of E_A may help explain the small difference in air stability between Ketolactam-1 and [60]PCBM despite the experimentally observed differences in LUMO energy. Electron transfer rates for a hopping process are determined by both the intersite coupling and the energetic offset between hopping sites. The combined contribution of both parameters defines the thermal activation energy for a hopping event. The relative electron transfer rates for fullerene-fullerene or fullerene-oxidant hopping will determine the degradation of n-channel transport in the thin-film. For fullerene-fullerene electron transfer, a higher E_A is required for hopping between Ketolactam-1 states relative to hopping between [60]PCBM states. Although the absolute value of localized site energies with respect to the vacuum level are deeper in Ketolactam-1, the expected energetic improvement in anionic stability is offset by the relative increase in the thermal energy required for the electron to hop to an adjacent fullerene. Although a deeper LUMO will reduce the hopping probability into trap states, our results suggest that energetic and spatial disorder may still influence stability.

IV. CONCLUSION

In summary, we have analyzed the properties of three soluble C_{60} derivatives. We have found reasonable agreement between theory and experiment used to determine trends in the electronic structure variations imposed by chemical modification of the parent carbon cage. Materials characterization suggests solid films of the fullerenes (prepared as described in the present report) show negligible differences in terms of crystallinity and hydrophobicity. The films were found to be suitable for supporting electron transport in OFETs. These OFETs could be used to assess the air stability of the electron transport in each fullerene. Although all three were found to be unstable in air, these measurements coupled with temperature-dependent charge transport studies suggest that the atmospheric stability of electron transporting n-channel materials depends not only on the absolute energy of hopping sites but also on the energetic disorder within the film. We suggest from these results that the energy required for hopping between fullerene sites relative to the energy for hopping into a trap state determines air stability. These studies may give insight for the atmospheric degradation mechanism of electron transport in fullerenes used in both electronic and optoelectronic devices.

ACKNOWLEDGMENTS

We are grateful to the Engineering and Physical Sciences Research Council (EPSRC), Research Councils UK (RCUK), and the Lee-Lucas Endowment for financial support. Work at Princeton University was supported by the Solvay Corporation and the National Science Foundation (DMR-1005892).

[1]B. Crone, A. Dodabalapur, Y.-Y. Lin, R. W. Filas, Z. Bao, A. La Duca, R. Sarpeshkar, H. E. Katz, and W. Li, Nature **403**, 521 (2000).
[2]X.-H. Zhang, W. J. Potscavage, Jr., S. Choi, and B. Kippelen, Appl. Phys. Lett. **94**, 043313 (2009).
[3]B. S. Ong, Y. Wu, P. Liu, and S. Gardner, J. Am. Chem. Soc. **126**, 3378 (2004).
[4]R. Hamilton, J. Smith, S. Ogier, M. Heeney, J. E. Anthony, I. McCulloch, J. Veres, D. D. C. Bradley, and T. D. Anthopoulos, Adv. Mater. **21**, 1166 (2008).
[5]H. Pan, Y. Li, Y. Wu, P. Liu, B. S. Ong, S. Zhu, and G. Xu, J. Am. Chem. Soc. **129**, 4112 (2007).
[6]C. Piliego, D. Jarzab, G. Gigli, Z. Chen, A. Facchetti, and M. A. Loi, Adv. Mater. **21**, 1573 (2009).
[7]H. Yan, Z. Chen, Y. Zheng, C. Newman, J. R. Quinn, F. Dötz, M. Kastler, and A. Facchetti, Nature **457**, 679 (2009).
[8]Y. Wen and Y. Lin, Adv. Mater. **22**, 1331 (2010).
[9]D. M. de Leeuw, M. M. J. Simenon, A. R. Brown, and R. E. F. Einerhand, Synth. Met. **87**, 53–59 (1997).
[10]B. A. Jones, A. Facchetti, M. R. Wasielewski, and T. J. Marks, J. Am. Chem. Soc. **129**, 15259 (2007).
[11]T. D. Anthopoulos, G. C. Anyfantis, G. C. Papavassiliou, and D. M. de Leeuw, Appl. Phys. Lett. **90**, 122105 (2007).
[12]H. Usta, C. Risko, Z. Wang, H. Huang, M. K. Deliomeroglu, A. Zhukovitskiy, A. Facchetti, and T. J. Marks, J. Am. Chem. Soc. **131**, 5586 (2009).
[13]R. T. Weitz, K. Amsharov, U. Zschieschang, M. Burghard, M. Jansen, M. Kelsch, B. Rhamati, P. A. van Aken, K. Kern, and H. Klauk, Chem. Mater. **21**, 4949 (2009).
[14]T. D. Anthopoulos, B. Singh, N. Marjanovic, N. S. Sariciftci, A. M. Ramil, H. Sitter, M. Cölle, and D. M. de Leeuw, Appl. Phys. Lett. **89**, 213504 (2006).
[15]X.-H. Zhang, B. Domercq, and B. Kippelen, Appl. Phys. Lett. **91**, 092114 (2007).
[16]C. Waldauf, P. Schilinsky, M. Perisutti, J. Hauch, and C. J. Brabec, Adv. Mater. **15**, 2084 (2003).
[17]T. D. Anthopoulos, D. M. de Leeuw, E. Cantatore, S. Setayesh, E. J. Meijer, C. Tanase, J. Hummelen, and P. W. M. Blom, Appl. Phys. Lett. **85**, 4205 (2004).
[18]M. Chikamatsu, S. Nagamatsu, Y. Yoshida, K. Saito, K. Yase, and K. Kikuchi, Appl. Phys. Lett. **87**, 203504 (2005).

[19]M. Chikamatsu, A. Itakura, Y. Yoshida, R. Azumi, and K. Yase, Chem. Mater. **20**, 7365 (2008).
[20]P. H. Wöbkenberg, J. Ball, D. D. C. Bradley, T. D. Anthopoulos, F. Kooistra, J. C. Hummelen, and D. M. de Leeuw, Appl. Phys. Lett. **92**, 143310 (2008).
[21]P. H. Wöbkenberg, D. D. C. Bradley, D. Kronholm, J. C. Hummelen, D. M. de Leeuw, M. Cölle, and T. D. Anthopoulos, Synth. Met. **158**, 468 (2008).
[22]S. P. Tiwari, X.-H. Zhang, W. J. Potscavage, Jr., and B. Kippelen, J. Appl. Phys. **106**, 054504 (2009).
[23]G. Yu, J. Gao, J. C. Hummelen, F. Wudl, and A. J. Heeger, Science **270**, 1789 (1995).
[24]N. Marjanovic, T. B. Singh, G. Dennler, S. Günes, H. Neugebauer, N. S. Sariciftci, R. Schwödiauer, and S. Bauer, Org. Electron. **7**, 188 (2006).
[25]H. Hoppe and N. S. Sariciftci, J. Mater. Chem. **16**, 45 (2006).
[26]B. C. Thompson and J. M. J. Fréchet, Angew. Chem. Int. Ed. **47**, 58 (2008).
[27]P. W. M. Blom, V. D. Mihailetchi, L. J. A. Koster, and D. E. Markov, Adv. Mater. **19**, 1551 (2007).
[28]P. A. Troshin, H. Hoppe, J. Renz, M. Egginer, J. Y. Mayorova, A. E. Goryachev, A. S. Peregudov, R. N. Lyubovskaya, G. Gobsch, N. S. Sariciftci, and V. F. Razumov, Adv. Funct. Mater. **19**, 779 (2009).
[29]P. Wei, J. H. Oh, G. Dong, and Z. Bao, J. Am. Chem. Soc. **132**, 8852 (2010).
[30]T. D. Anthopoulos, F. B. Kooistra, H. J. Wondergem, D. Kronholm, J. C. Hummelen, and D. M. de Leeuw, Adv. Mater. **18**, 1679 (2006).
[31]C. J. Brabec, A. Cravino, D. Meissner, N. S. Sariciftci, T. Fromherz, M. T. Rispens, L. Sanchez, and J. C. Hummelen, Adv. Funct. Mater. **11**, 374 (2001).
[32]M. Lenes, G. A. H. Wetzelaer, F. B. Kooistra, S. C. Veenstra, J. C. Hummelen, and P. W. M. Blom, Adv. Mater. **20**, 2116 (2008).
[33]M. Lenes, S. W. Shelton, A. B. Sieval, D. F. Kronholm, J. C. Hummelen, and P. W. M. Blom, Adv. Funct. Mater. **19**, 3002 (2009).
[34]J. M. Frost, M. A. Faist, and J. Nelson, Adv. Mater. (submitted).
[35]R. K. M. Bouwer and J. C. Hummelen, Chem.-Eur. J. **16**, 11250 (2010).
[36]M. Bühl and A. Hirsch, Chem. Rev. **101**, 1153 (2001).
[37]B. W. D'Andrade, S. Datta, S. R. Forrest, P. Djurovich, E. Polikarpov, and M. E. Thompson, Org. Electron. **6**, 11 (2005).
[38]K. Akaike, K. Kanai, H. Yoshida, J. Tsutsumi, T. Nishi, N. Sato, Y. Ouchi, and K. Seki, J. Appl. Phys. **104**, 023710 (2008).
[39]C. Müller, T. A. M. Ferenczi, M. Campoy-Quiles, J. M. Frost, D. D. C. Bradley, P. Smith, N. Stingelin-Stutzmann, and J. Nelson, Adv. Mater. **20**, 3510 (2008).
[40]J. Zhao, A. Swinnen, G. V. Assche, J. Manca, D. Vanderzande, and B. V. Mele, J. Phys. Chem. B **113**, 1587 (2009).
[41]K. Terada and H. Muta, Jpn. J. Appl. Phys. **18**, 953 (1979).
[42]E. J. Meijer, G. H. Gelinck, E. van Veenendaal, B.-H. Huisman, D. M. de Leeuw, and T. M. Klapwijk, Appl. Phys. Lett. **82**, 4576 (2003).
[43]Y. Shen, A. R. Hosseini, M. H. Wong, and G. G. Malliaras, Chem. Phys. Chem. **5**, 16 (2004).
[44]J. C. Scott, J. Vac. Sci. Technol. A **21**, 521 (2003).
[45]J. H. Cho, D. H. Kim, Y. Jang, W. H. Lee, K. Ihm, J.-H. Han, S. Chung, and K. Cho, Appl. Phys. Lett. **89**, 132101 (2006).
[46]J. K. J. van Duren, V. D. Mihailetchi, P. W. M. Blom, T. van Woudenbergh, J. C. Hummelen, M. T. Rispens, R. A. J. Janssen, and M. M. Wienk, J. Appl. Phy. **94**, 4477 (2003).
[47]T. D. Anthopoulos, D. M. de Leeuw, E. Cantatore, P. van't Hof, J. Alma, and J. C. Hummelen, J. Appl. Phys. **98**, 054503 (2005).
[48]N. I. Craciun, J. Wildeman, and P. W. M. Blom, Phys. Rev. Lett. **100**, 056601 (2008).
[49]I. I. Fishchuk, A. K. Kadaschchuk, J. Genoe, M. Ullah, H. Sitter, T. B. Singh, N. S. Sariciftci, and H. Bässler, Phys. Rev. B **81**, 045202 (2010).